Electron-magnon spin conversion and magnonic spin pumping in an antiferromagnet/heavy metal heterostructure

Xi-guang Wang,[1] Yao-Zhuang Nie,[1] L. Chotorlishvili,[2] Qing-lin Xia,[1] J. Berakdar,[2] and Guang-hua Guo[1,*]
[1]*School of Physics and Electronics, Central South University, Changsha 410083, China*
[2]*Institut für Physik, Martin-Luther Universität Halle-Wittenberg, D-06120 Halle/Saale, Germany*

(Received 18 September 2019; revised 21 December 2020; accepted 25 January 2021; published 3 February 2021)

We study the exchange between electron and magnon spins at the interface of an antiferromagnet and a heavy metal at finite temperatures. The underlying physical mechanism is based on spin torque associated with the creation/annihilation of thermal magnons with right-hand and left-hand polarization. The creation/annihilation process depends strongly on the relative orientation between the polarization of the electron and the magnon spins. For a sufficiently strong spin-transfer torque (STT), the conversion process becomes nonlinear, generating a nonzero net spin pumping current in the antiferromagnet that can be detected in the neighboring metal layer. Applying an external magnetic field renders possible the manipulation of the STT driving thermal spin pumping. Our theoretical results are experimentally feasible and are of a direct relevance to antiferromagnet-based spintronic devices.

DOI: 10.1103/PhysRevB.103.064404

I. INTRODUCTION

Electronic and magnonic spin currents are central to spintronics [1–6]. Electronic spin current is generated, for instance, due to the spin Hall effect (SHE) in a nonmagnetic metal layer [5,7–9] or through the oscillation of magnetization in a ferromagnetic layer (spin pumping) [10–13]. The magnonic spin current, meaning a flux of nonequilibrium magnons, results from an applied temperature gradient, microwave field, or due to electronic spin-transfer torque [2,14–19]. Spin currents in antiferromagnets (AFMs) are also highly interesting for AFM spintronics [20–24]. Several spin transport phenomena, including SHE, spin Seebeck effect, and Néel spin-orbit torque were reported, and their potential for applications was discussed in AFMs [20–30]. Of a particular interest is the behavior of a magnonic spin current flowing from a ferromagnet (FM) across an insulating AFM layer [27,31–37], which offers a way for integration of magnonic spintronic and AFM devices allowing to act on the AFM by exciting the FM layer [27].

AFM hosts two degenerate magnon modes with opposite angular momenta. The generation of magnonic spin current entails a symmetry break between modes [22,27,38]. The degeneracy can be lifted by different means: external magnetic field [26,29], and interlayer exchange interaction from a neighboring FM layer [27,27,32,39,40]. All these methods lead to a nonzero net magnonic spin current flowing in the AFM. Magnonic spin currents are usually excited by a temperature gradient (spin Seebeck effect) or microwave field pumping. However, the thermal gradient is relatively slow for a swift on-and-off dynamical switching of magnonic spin current, while microwave field pumping is energetically costly. The direct conversion between an electronic charge signal and a magnonic signal is advantageous for designing viable AFM magnonic devices.

Recent studies uncover the possibility of electronic/magnonic spin current conversion [36,41], indicating that the spin accumulation at a nonmagnetic metal/AFM interface can break the degenerate magnon modes, leading to a magnonic spin current with no external magnetic field or thermal gradient [41]. The mechanism was corroborated experimentally [36]. The effect depends linearly on the spin accumulation amplitude and can be controlled by applying an external magnetic field. A substantial enhancement was observed at the magnetic-field-induced spin-flop transition. In the present work we explore finite-temperature magnonic excitations and develop a theoretical approach for a finite and uniform temperature electronic/magnonic spin conversion in the heavy metal/AFM insulator heterostructure. The calculations based on our model offer an explanation of the experimental results. In particular, we show that the magnonic spin pumping signal is maximal for the Néel order parallel to the spin accumulation. The present work proves that due to finite-temperature magnonic excitations in AFM, the electronic spin current in heavy metal (HM) can traverse through the insulating AFM layer. In our model, not FM but the AFM layer plays the role of the spin-current tunnel junction. We sandwich the AFM layer between two HM layers, meaning we consider a HM/insulating AFM/HM heterostructure. At finite temperatures, the electronic spin current creates (annihilates) thermal magnons with spin polarization opposite (parallel) to the polarization of the electron spin. Thus, spins of the electrons from the HM layer are efficiently converted to AFM magnons. The induced magnon spins are further delivered to the second HM layer and eventually are converted back to the electron spin current via the spin pumping effect. The effectiveness of the spin transport via magnons depends on

*guogh@mail.csu.edu.cn

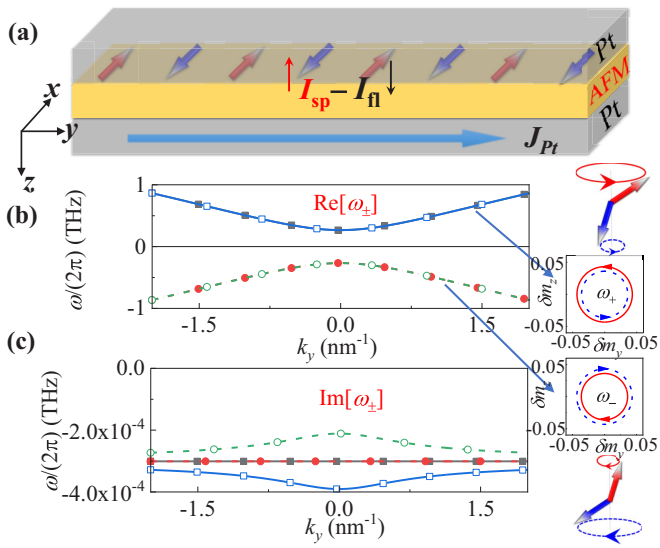

FIG. 1. (a) Schematics of the studied heterostructure. The insulating antiferromagnet is sandwiched between two HMs (here, Pt). A charge current with density $J_{\rm Pt}$ flows in one of the metal layers. The pure electron spin current generated through the spin Hall effect is denoted by its spin polarization direction $\boldsymbol{\mu}_s^N = -\mathbf{z} \times \mathbf{j}_{\rm Pt}$. (b) Dispersion relations (i.e., real parts) and (c) imaginary parts of eigenfrequencies ω_+ (squares) and ω_- (circles), with ($c_J = 0.0001$ THz, open dots) and without STT ($c_J = 0$, solid dots). Bottom right panel shows the magnon precession trajectories in the y-z plane for $k_y = 0$. Magnons are excited by a microwave field $\boldsymbol{\omega}_H = (0, h_y, h_z)e^{(ik_y y - i\omega t)}$ with $h_y = 3 \times 10^{-4}$ THz, $h_z = 3 \times 10^{-4} i$ THz, and $\omega = \mathrm{Re}[\omega_\pm]$. Red and blue arrows represent the sublattice magnetizations $\mathbf{m}_1$ and $\mathbf{m}_2$, respectively.

the electronic spin current and on the external magnetic field. Due to the influence akin to spin-transfer torque (STT) on the effective damping of two magnon modes, the spin transport depends nonlinearly on the electronic spin current, when the amplitude of STT is large.

The paper is organized as follows: In Sec. II we specify the model, in Sec. III we analyze the polarization of magnons and derive the magnon eigenmodes, and in Sec. IV we explore the effect of STT. The thermal and spin pumping effects we discuss in Sec. IV. In Secs. VI and VII we discuss the effect of external magnetic fields, and we conclude with Sec. VIII.

II. THEORETICAL MODEL

The structure considered in this study is shown in Fig. 1(a). The AFM layer is sandwiched between two HMs. A charge current with density J_{Pt} passes through one metal and induces a transversal spin current due to the spin Hall effect. The electronic spin current is converted into a magnonic spin current at the AFM/HM interface via the SHE-based STT [30,42]. The magnonic spin current is detected in the second metal via the spin pumping effect [34,35,43–45].

To describe the magnetization dynamics in the AFM, we introduce the average magnetization vector $\mathbf{m} = (\mathbf{m}_1 + \mathbf{m}_2)/2$ and the Néel vector $\mathbf{n} = (\mathbf{m}_1 - \mathbf{m}_2)/2$. Here, $\mathbf{m}_1$ and $\mathbf{m}_2$ represent sublattice magnetizations of the AFM under the constraints $|\mathbf{m}|^2 + |\mathbf{n}|^2 = 1$ and $\mathbf{m} \cdot \mathbf{n} = 0$. The dynamics of $\mathbf{m}$ and $\mathbf{n}$ are governed by the stochastic Landau-Lifshitz-Gilbert (LLG) equations with STTs [44]:

$$\begin{aligned} \partial_t \mathbf{m} &= \tfrac{1}{2}(\boldsymbol{\omega}_m \times \mathbf{m} + \boldsymbol{\omega}_n \times \mathbf{n}) + \boldsymbol{\tau}_m^T + \boldsymbol{\tau}_m^{\rm GD} + \boldsymbol{\tau}_m^{\rm STT}, \\ \partial_t \mathbf{n} &= \tfrac{1}{2}(\boldsymbol{\omega}_m \times \mathbf{n} + \boldsymbol{\omega}_n \times \mathbf{m}) + \boldsymbol{\tau}_n^T + \boldsymbol{\tau}_n^{\rm GD} + \boldsymbol{\tau}_n^{\rm STT}. \end{aligned} \quad (1)$$

The frequencies $\boldsymbol{\omega}_m$ and $\boldsymbol{\omega}_n$ represent the effective fields and are defined through $\boldsymbol{\omega}_m = -\frac{\gamma}{M_s}\frac{\delta E_{\rm AFM}}{\delta \mathbf{m}}$ and the $\boldsymbol{\omega}_n = -\frac{\gamma}{M_s}\frac{\delta E_{\rm AFM}}{\delta \mathbf{n}}$. The free energy density [46] $E_{\rm AFM}$ has the form

$$\begin{aligned} E_{\rm AFM} = \frac{M_s}{\gamma}\Big\{ &\omega_E(\mathbf{m}^2 - \mathbf{n}^2) - a^2\frac{\omega_E}{4}[(\nabla \mathbf{m})^2 - (\nabla \mathbf{n})^2] \\ &- 2\boldsymbol{\omega}_H \cdot \mathbf{m} - \omega_A\big(m_x^2 + n_x^2\big)\Big\}, \end{aligned} \quad (2)$$

where ω_E is the exchange frequency, ω_A is the easy-axis (along x) anisotropy frequency, $\boldsymbol{\omega}_H$ is the frequency describing the external magnetic field, and a is the length of the antiferromagnetic unit cell. In the stochastic LLG equations (1), the temperature is introduced by the thermal random magnetic field torque:

$$\begin{aligned} \boldsymbol{\tau}_m^T &= \mathbf{h}_m \times \mathbf{m} + \mathbf{h}_n \times \mathbf{n}, \\ \boldsymbol{\tau}_n^T &= \mathbf{h}_m \times \mathbf{n} + \mathbf{h}_n \times \mathbf{m}. \end{aligned} \quad (3)$$

The Gilbert damping torques are given through

$$\begin{aligned} \boldsymbol{\tau}_m^{\rm GD} &= \alpha(\mathbf{m} \times \partial_t \mathbf{m} + \mathbf{n} \times \partial_t \mathbf{n}), \\ \boldsymbol{\tau}_n^{\rm GD} &= \alpha(\mathbf{m} \times \partial_t \mathbf{n} + \mathbf{n} \times \partial_t \mathbf{m}), \end{aligned} \quad (4)$$

and the STTs read

$$\begin{aligned} \boldsymbol{\tau}_m^{\rm STT} &= c_J\big(\mathbf{m} \times \boldsymbol{\mu}_s^N \times \mathbf{m} + \mathbf{n} \times \boldsymbol{\mu}_s^N \times \mathbf{n}\big), \\ \boldsymbol{\tau}_n^{\rm STT} &= c_J\big(\mathbf{n} \times \boldsymbol{\mu}_s^N \times \mathbf{m} + \mathbf{m} \times \boldsymbol{\mu}_s^N \times \mathbf{n}\big). \end{aligned} \quad (5)$$

Here α is the Gilbert damping constant, the strength of STT is quantified through $c_J = \frac{2\gamma\hbar\theta_{\rm SH}\lambda G_r \tanh(d_{\rm Pt}/2\lambda) J_{\rm Pt}}{e\mu_0 d_{\rm AF} M_s[\sigma + 2\lambda G_r \coth(d_{\rm Pt}/\lambda)]}$ [47,48], thermal fields $\mathbf{h}_m$ and $\mathbf{h}_n$ satisfy the time correlation [49] $\langle h_{m,p}(\mathbf{r}, t) h_{m,q}(\mathbf{r}', t')\rangle = \langle h_{n,p}(\mathbf{r}, t) h_{n,q}(\mathbf{r}', t')\rangle = \delta_{pq}\delta(t - t')$ $\delta(\mathbf{r} - \mathbf{r}')\sigma_T^2$, and $\sigma_T^2 = \frac{\alpha\gamma k_B T}{\mu_0 M_s V}$ describes the amplitude of the random field. $\boldsymbol{\mu}_s^N = (1, 0, 0)$ represents the electron spin polarization, $J_{\rm Pt}$ is the electric current density, $\theta_{\rm SH}$ is the spin Hall angle, σ is the electric conductivity, λ is the spin diffusion length, G_r is the spin mixing interface conductance per unit area, $d_{\rm Pt}$ and $d_{\rm AF}$ are the thicknesses of Pt and AFM, k_B is the Boltzmann constant, T is the temperature, V is the volume of AFM, γ is the gyromagnetic ratio, M_s is the saturation magnetization of the sublattice, and $p, q = x, y, z$. In what follows, we consider electric current density below the threshold value needed for excitation of magnetization auto-oscillations [42,50]. Therefore we exploit a finite uniform temperature thermal bath as an energy supply to compensate damping processes and generate magnonic excitations.

III. MAGNON POLARIZATION

To construct an analytic model for describing the propagation of magnons in the AFM we consider slight derivations from the stable state [$\mathbf{m}_0 = (0, 0, 0)$ and $\mathbf{n}_0 = (1, 0, 0)$], $\mathbf{m} = \mathbf{m}_0 + (0, \delta m_y, \delta m_z)$, and $\mathbf{n} = \mathbf{n}_0 + (0, \delta n_y, \delta n_z)$. The

eigensolutions of the linearized equation (1) have the form $\delta m_p = X_p e^{i(k_y y-\omega t)}$ and $\delta n_p = Y_p e^{i(k_y y-\omega t)}$, where $p = y, z$. We insert $\mathbf{m}$ and $\mathbf{n}$ into Eq. (1) and obtain the equation $i\partial_t \boldsymbol{\psi} = \hat{H}\boldsymbol{\psi}$ for the vector $\boldsymbol{\psi} = (X_y, X_z, Y_y, Y_z)$. With the definitions of the frequencies $\omega_k = 2\omega_E + \omega_A - \frac{a^2\omega_E k_y^2}{4}$ and $\omega_{ak} = \omega_A + \frac{a^2\omega_E k_y^2}{4}$, the Hamiltonian $\hat{H}$ (without external excitation) reads

$$\hat{H} = \begin{pmatrix} -i\alpha\omega_k & i\alpha c_J & -ic_J & -i\omega_{ak} \\ -i\alpha c_J & -i\alpha\omega_k & i\omega_{ak} & -ic_J \\ -ic_J & -i\omega_k & -i\alpha\omega_{ak} & i\alpha c_J \\ i\omega_k & -ic_J & -i\alpha c_J & -i\alpha\omega_{ak} \end{pmatrix}. \tag{6}$$

From this Hamiltonian two eigenfrequencies $\omega_\pm$ follow:

$$\omega_\pm = \pm\sqrt{(\omega_{ak} - ic_J)(\omega_k - ic_J) - \alpha^2\left(\omega_E - \frac{a^2\omega_E k_y^2}{4}\right)^2} - \alpha c_J - i\alpha(\omega_{ak} + \omega_k)/2. \tag{7}$$

The spin-wave modes $\omega_\pm$ correspond to the opposite circular polarizations. Without STT ($c_J = 0$), the two magnon modes are degenerate, and the magnon dispersion relations $\mathrm{Re}[\omega_\pm] = \pm\sqrt{\omega_{ak}\omega_k - \alpha^2(\omega_E - \frac{a^2\omega_E k_y^2}{4})^2}$ of the two modes are symmetric with respect to $\omega = 0$. Using MnF_2 as a material with the parameters $\omega_E = 9.3 \times 10^{12}\,\mathrm{s}^{-1}$, $\omega_A = 1.5 \times 10^{11}\,\mathrm{s}^{-1}$, $M_s = 48000$ A/m, $\alpha = 0.0002$, and $a = 4.1$ Å, we calculated numerically the degenerate modes $\omega_\pm$ for $c_J = 0$. The results are shown in Figs. 1(b) and 1(c).

To explore the polarization of the two magnon modes, we apply the microwave filed $\boldsymbol{\omega}_H = (0, h_y, h_z)e^{(ik_y y-i\omega t)}$. The excited magnon amplitudes are extracted analytically from the linearized equation (1) as

$$\begin{aligned} X_y &= \frac{(h_y + ih_z)(-ic_J - \omega_{ak} + i\alpha\omega)}{l_+^\omega} - \frac{(h_y - ih_z)(-ic_J + \omega_{ak} - i\alpha\omega)}{l_-^\omega}, \\ X_z &= \frac{(-ih_y + h_z)(-ic_J - \omega_{ak} + i\alpha\omega)}{l_+^\omega} - \frac{(ih_y + h_z)(-ic_J + \omega_{ak} - i\alpha\omega)}{l_-^\omega}, \\ Y_y &= \frac{(h_y + ih_z)\omega}{l_+^\omega} - \frac{(h_y - ih_z)\omega}{l_-^\omega}, \quad Y_z = \frac{(-ih_y + h_z)\omega}{l_+^\omega} - \frac{(ih_y + h_z)\omega}{l_-^\omega}, \end{aligned} \tag{8}$$

with $l_\pm^\omega := 2\omega^2 + 2[-c_J \pm i(\omega_{ak} - i\alpha\omega)][-c_J \pm i(\omega_k - i\alpha\omega)]$. Excited by the microwave field, the local magnetization precesses around the equilibrium state. The precessions of the two sublattices are demonstrated in the bottom right panel in Fig. 1 for the case $k_y = 0$. The magnons of the two modes $\omega_\pm$ have opposite chirality. For the mode ω_+, the magnons of both $\mathbf{m}_1$ and $\mathbf{m}_2$ sublattices precess around $+\mathbf{x}$ direction counterclockwise, meaning that the right-hand polarized magnon (identified with $\mathbf{m}_1$) is coupled to left-hand magnon (identified with $\mathbf{m}_2$), and the amplitude of magnons for $\mathbf{m}_1$ is larger. For the ω_- mode, the circular polarizations of both magnons are reversed (clockwise precession around $+x$) and the amplitude of the right-hand magnons for $\mathbf{m}_2$ is larger.

IV. EFFECT OF STT

The influence of the SHE-induced STT on the eigenfrequencies $\omega_\pm$ is shown in Figs. 1(b) and 1(c). The changes due to STT in the real parts of $\omega_\pm$ are negligible. STT with $c_J > 0$ (i.e., electron polarization points along the $+x$ direction), increases $\mathrm{Im}[\omega_+]$, meaning that the attenuation of this mode is enhanced. On the other hand, $\mathrm{Im}[\omega_-]$ decreases, and the attenuation is weakened. The change in $\mathrm{Im}[\omega]$ depends linearly on c_J [Fig. 2(a)], and $\mathrm{Im}[\omega_+]$ ($\mathrm{Im}[\omega_-]$) is decreased (increased) by reversing the STT ($c_J < 0$).

The STT also affects the magnon excitation efficiency. Using a polarized microwave field $\boldsymbol{\omega}_H = (0, h_y, h_z)e^{(ik_y y-i\omega t)}$ ($h_y = 3 \times 10^{-4}$ THz, $h_z = 3i \times 10^{-4}$ THz, $k_y = 0$, and $\omega = \mathrm{Re}[\omega_\pm]$) and Eq. (8), we calculate amplitudes of the excited magnetization oscillations, see Fig. 2. Apparently the positive (negative) c_J decreases (increases) the efficiency of exciting magnons of the ω_+ mode. The effect is reversed for the ω_- mode. In view of the changes in the imaginary parts of eigenfrequencies [Fig. 2(a)], we conclude that the effectiveness of the exciting magnon increases if the imaginary parts of $\omega_\pm$ are decreased, i.e., the effective magnon damping α_{eff} is lowered.

Enhancement and annihilation of magnons due to the STT are asymmetric and nonlinear, and the increase of the magnon amplitude is much stronger. This finding is in line with the STT-induced magnon enhancement/annihilation in FM, where the enhancement (annihilation) occurs when electron polarization is opposite (parallel) to the magnon polarization and decreases (increases) the magnon effective damping [17,48].

V. THERMAL EFFECT AND SPIN PUMPING

From Eq. (1) we infer that the thermal magnons are excited by the thermal random fields $\mathbf{h}_m$ and $\mathbf{h}_n$. By solving the dynamic equations, we obtain the dynamic magnetic susceptibility matrix $\hat{\chi}(\omega)$, and $l_p(\omega) = \sum_q \chi_{pq} h_q(\omega)$ with $l_1 = m_y$,

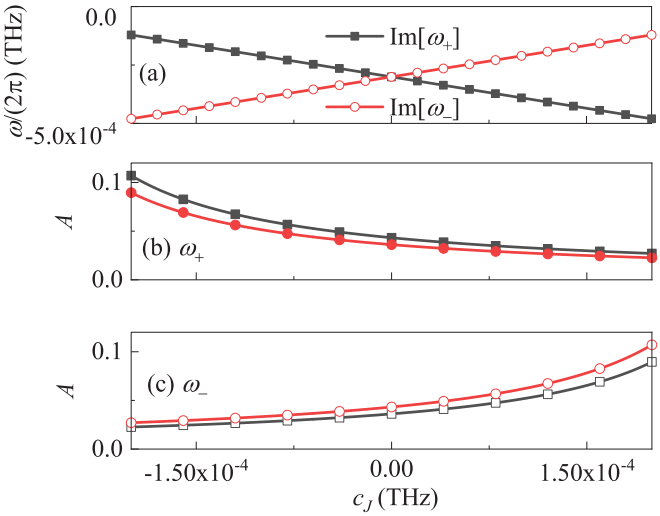

FIG. 2. (a) c_J dependence of the imaginary parts of eigenfrequencies $\omega_\pm$ at $k_y = 0$. (b,c) Excited by $\boldsymbol{\omega}_H = (0, h_y, h_z)e^{(ik_y y - i\omega t)}$ with $h_y = 3 \times 10^{-4}$ THz, $h_z = 3i \times 10^{-4}$ THz, and $k_y = 0$, c_J dependence of excited oscillation amplitude for (b) $\omega = \mathrm{Re}[\omega_+]$ and (c) $\omega = \mathrm{Re}[\omega_-]$. Solid squares and open circles are respectively the amplitudes of the sublattice magnetization, $\mathbf{m}_1$ and $\mathbf{m}_2$.

$l_2 = m_z$, $l_3 = n_y$, $l_4 = n_z$, $h_1 = h_{m,y}$, $h_2 = h_{m,z}$, $h_3 = h_{n,y}$, and $h_4 = h_{n,z}$):

$$\hat{\chi} = \begin{pmatrix} \frac{c_-}{l_+} - \frac{c_+}{l_-} & \frac{ic_-}{l_+} + \frac{ic_+}{l_-} & \frac{\omega}{l_+} - \frac{\omega}{l_-} & \frac{i\omega}{l_+} + \frac{i\omega}{l_-} \\ -\frac{ic_-}{l_+} - \frac{ic_+}{l_-} & \frac{c_-}{l_+} - \frac{c_+}{l_-} & -\frac{i\omega}{l_+} - \frac{i\omega}{l_-} & \frac{\omega}{l_+} - \frac{\omega}{l_-} \\ \frac{\omega}{l_+} - \frac{\omega}{l_-} & \frac{i\omega}{l_+} + \frac{i\omega}{l_-} & \frac{d_-}{l_+} - \frac{d_+}{l_-} & \frac{id_-}{l_+} + \frac{id_+}{l_-} \\ -\frac{i\omega}{l_+} - \frac{i\omega}{l_-} & \frac{\omega}{l_+} - \frac{\omega}{l_-} & -\frac{id_-}{l_+} - \frac{id_+}{l_-} & \frac{d_-}{l_+} - \frac{d_+}{l_-} \end{pmatrix}, \tag{9}$$

where $c_\pm := -ic_J \pm (\omega_{ak} - i\alpha\omega)$, and $d_\pm := -ic_J \pm (\omega_k - i\alpha\omega)$.

By virtue of spin pumping, the magnetization dynamics in the AFM can pump into the neighboring metal layer the spin current [43,44]

$$\mathbf{I}_{sp} = \frac{\hbar g_r}{2\pi}(\mathbf{m} \times \partial_t \mathbf{m} + \mathbf{n} \times \partial_t \mathbf{n}). \tag{10}$$

Here, $g_r = G_r h/e^2$ is the rescaled interface mixing conductance. In contrast to spin pumping current, the fluctuation spin current $\mathbf{I}_{fl} = -\frac{2M_s}{\gamma}(\mathbf{m} \times \mathbf{h}'_m + \mathbf{n} \times \mathbf{h}'_n)$ flows back to the AFM [49]. $\mathbf{h}'_m$ and $\mathbf{h}'_n$ satisfy the time correlation $\langle h'_{m,p}(\mathbf{r}, t)h'_{m,q}(\mathbf{r}', t')\rangle = \langle h'_{n,p}(\mathbf{r}, t)h'_{n,q}(\mathbf{r}', t')\rangle = \delta_{pq}\delta(t - t')\delta(\mathbf{r} - \mathbf{r}')\frac{\alpha'\gamma k_B T}{\mu_0 M_s V}$, and $\alpha' = \gamma\hbar g_r/(4\pi M_s V)$. The net spin current injected into the neighboring metal is $\mathbf{I}_s = \mathbf{I}_{sp} + \mathbf{I}_{fl}$. Then, with the magnon dynamics described by Eq. (9), the time derivative of the correlation function for $\mathbf{I}_{sp}$ within the macrospin model ($k_y = 0$) is

$$\langle \dot{l}_p l_q \rangle = \sigma_T^2 \int i\omega \sum_n \chi_{pn}(\omega)\chi_{qn}(-\omega)\frac{d\omega}{2\pi}, \tag{11}$$

where $p, q, n = 1, 2, 3, 4$. Using the contour integration method, we derive the finite x component of the spin current

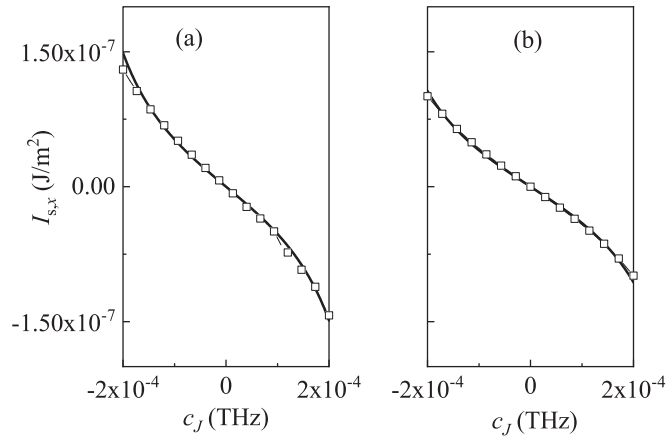

FIG. 3. c_J dependence of net current $\langle I_{s,x}\rangle$ at $T = 30$ K for (a) macrospin and (b) 1D models. Analytical (solid lines) and numerically simulated (open dots) results are shown.

$I_{sp,x}$ as

$$\langle I_{sp,x}\rangle = \frac{\hbar g_r \sigma_T^2 c_J(\omega_{ak} + \omega_k)}{2\pi(c_J^2 - \alpha^2\omega_{ak}\omega_k)}. \tag{12}$$

The two other components of the spin current vanish $\langle I_{sp,y}\rangle = \langle I_{sp,z}\rangle = 0$. The above equation indicates that the spin pumping current's polarization is parallel to the electron polarization and the equilibrium Néel order vector. Without STT, two degenerate magnon modes are equally excited by thermal fluctuation, and the pumping current $\langle I_{sp,x}\rangle = 0$. Below the critical value $c_J < \alpha\sqrt{\omega_A\omega_k}$ (above which the STT changes the stable state), positive c_J creates the negative $\langle I_{sp,x}\rangle$. The reason is that positive c_J enhances the ω_- mode polarized towards $-x$ (generating negative pumping current) but weakens the ω_+ mode polarized towards $+x$ (generating positive pumping current). The sign of $\langle I_{sp,x}\rangle$ changes with reversing the direction of the electric current (the sign of c_J). The change of the magnon density induced by STT is nonlinear (see Fig. 2), and therefore the amplitude of $\langle I_{sp,x}\rangle$ also changes nonlinearly with c_J. The fluctuating spin current vanishes $\mathbf{I}_{fl} = 0$. Thus the net current is equal to the spin pumping current $\langle I_{s,x}\rangle = \langle I_{sp,x}\rangle$. Numerical results calculated from Eq. (12) are shown in Fig. 3(a) and support the analytical findings. These findings are in line with earlier theoretical predictions based on fluctuation-dissipation theorems [36,41]. Previous works showed that the spin accumulation generates linear spin current without an external magnetic field and thermal gradient. The emphasis here is on nonlinearities due to a large spin-polarized charge current and the implications for the effective magnon damping and magnonic spin current (as discussed in Sec. IV).

We extended the results obtained for the single macrospin model to the spatially inhomogeneous dynamical modes (i.e., excited finite wave vector $\mathbf{k}$) and obtain the time derivative of the correlation function $\mathbf{I}_{sp}$:

$$\langle \dot{l}_p l_q \rangle = \sigma_T^2 S_\zeta \int \frac{d^\zeta \mathbf{k}}{(2\pi)^\zeta} \int i\omega \sum_n \chi_{pn}(\omega, \mathbf{k})\chi_{qn}(-\omega, -\mathbf{k})\frac{d\omega}{2\pi}. \tag{13}$$

Here, $\zeta = 1$ is for the one-dimensional (1D) model ($\mathbf{k} = k_y\mathbf{e}_y$, and S_1 is the sample length along y). For the two-dimensional (2D) model $\zeta = 2$ ($\mathbf{k} = k_x\mathbf{e}_x + k_y\mathbf{e}_y$, and $S_2 = S_{xy}$ is the area of the sample plane).

Due to the limited size of discrete unit cell, the value of the magnon wave vector cannot be too large. We integrate Eq. (13) in the finite range of $-k_c < k_{x,y} < k_c$ with $k_c = \pi/l_y$, where l_y is the unit cell size. For a 1D model, we infer

$$\langle I_{sp,x}\rangle = \hbar g_r \sigma_T^2 l_y c_J(\omega_A + \omega_E) \times \frac{\left[\omega_{j+}\text{atan}\left(\frac{\alpha a k_c\sqrt{\omega_E}}{2\omega_{j-}}\right) - \omega_{j-}\text{atan}\left(\frac{\alpha a k_c\sqrt{\omega_E}}{2\omega_{j+}}\right)\right]}{2\pi^2\omega_{j+}\omega_{j-}\sqrt{\alpha^2(\omega_A+\omega_E)^2 - c_J^2}}, \tag{14}$$

with

$$\omega_{j\pm} = \sqrt{\alpha(\pm\sqrt{\alpha^2(\omega_A+\omega_E)^2 - c_J^2} - \alpha\omega_E)}. \tag{15}$$

If STT is applied $c_J \neq 0$, the variation of $\langle I_{sp,x}\rangle$ for 1D model is similar to that for macrospin, including the aspects of sign and nonlinearity, as confirmed by numerical calculations in Fig. 3(b).

To quantify the effectiveness of the above conversion process, we compare the difference between the injected electronic spin current and output magnonic pumping current. The impact of the spin-transfer torque on the magnetization dynamics is proportional to the electronic spin current flowing inside the attached heavy metal layer, i.e., the spin-transfer torque amplitude $c_J = -\frac{\gamma J_s}{\mu_0 d_{AF} M_s}$ [51–54]. Here $J_s = S\theta_{\text{SH}}\frac{\hbar}{2e}J_H$ is the electronic spin current density in a heavy meal layer, J_H is the charge current density, θ_{SH} is the spin Hall angle, S is the transparency at the interface, and μ_0 is the vacuum permeability. For $c_J = 2\times10^{-4}$ THz one finds an electronic spin current density $J_s = -\frac{c_J\mu_0 d_{AF}M_s}{\gamma} = -2.73\times10^{-7}$ J/m^2. The magnonic spin current density reaches -1.47×10^{-7} J/m^2 (see Fig. 3), and the conversion efficiency is estimated to be $(-1.47\times10^{-7})/(-2.73\times10^{-7}) = 54\%$.

To support the analytical results, we numerically solved for the LLG Eqs. (1). In the numerical simulation the spin pumping current's value is determined from the expression Eq. (10). Under the same parameters adopted above, we compare the simulation results with the analytical calculations in Fig. 3, confirming the value of the analytical expressions. The thickness of AFM used in the numerical simulation is $d_{AF} = 5$ nm. We also consider the influence of the finite width of AFM, and the AFM sample with a thickness of $d_{AF} = 5$ nm and width 100 nm. The result is shown in Fig. 4. The STT-induced magnonic pumping current is still antisymmetric concerning the electric current direction, and the nonlinear trend becomes weaker as compared with the results in Fig. 3. In addition, we consider the case with the electron spin polarization $\boldsymbol{\mu}_s^N = (0, 1, 0)$ being perpendicular to the equilibrium Néel order vector $\mathbf{n}_0$. Our calculations show that the STT does not affect the magnons in the AFM in this case, and therefore $\langle I_{sp,x}\rangle = 0$. This conclusion is confirmed also by the numerical simulation.

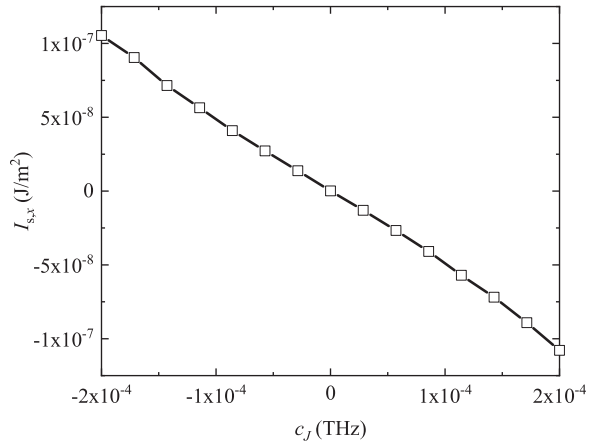

FIG. 4. Numerically simulated c_J dependence of net current $\langle I_{s,x}\rangle$ at $T = 30$ K for AFM film with finite width 100 nm.

VI. APPLYING MAGNETIC FIELD ALONG *x*

An applied magnetic field impacts the magnon polarization and leads to the nontrivial phenomena of electron-magnon spin conversion in the AFM/heavy heterostructure. Here, we mainly consider the case with the external magnetic field ω_{Hx} applied along the easy axis (x axis) for $\omega_{Hx} < \sqrt{2\omega_E\omega_A} = 1.7$ THz. In this range, the linear antiparallel structure [$\mathbf{m}_0 = (0, 0, 0)$ and $\mathbf{n}_0 = (1, 0, 0)$] is stable. In the same manner we obtain the eigenfrequencies $\omega_\pm$:

$$\omega_\pm = \pm\sqrt{F_\pm} + \omega_{ch} - \frac{i\alpha}{2}\omega_{ck}^+, \tag{16}$$

where

$$\begin{aligned} F_\pm = \frac{1}{2\omega_{ch}}\big(&- 4c_J^2\omega_{Hx} + \alpha^3 c_J\big[4\omega_{Hx}^2 + (\omega_{ck}^-)^2\big] \\ &+ \alpha^2\omega_{Hx}\big[8c_J^2 - 4\omega^2 - (\omega_{ck}^-)^2\big] + 4\omega_{Hx}\omega_k\omega_A \\ &- 4ic_j\omega_{ch}\omega_{ck}^+ + 4\alpha\big[c_J^3 - i\omega_{Hx}\omega_{ch}\omega_{ck}^+ \\ &- c_J(2\omega_{Hx}^2 + \omega_k\omega_{ak})\big]\big), \end{aligned} \tag{17}$$

where $\omega_{ch} = \omega_{Hx} - \alpha c_J$, and $\omega_{ck}^\pm = \omega_k \pm \omega_{ak}$. For the parameters considered above, we calculate the magnon dispersion relations [Figs. 5(a) and 5(b)]. The real parts of both modes ω_+ and ω_- are shifted upward, and the values of the corresponding imaginary parts are changed, steering the separation between Im[$\omega_\pm$]. These changes increase linearly with ω_{Hx}, as demonstrated in Figs. 5(c) and 5(d). STT affects mainly the imaginary parts, and Im[ω_+] (Im[ω_-]) is increased (decreased) by a positive c_J (cf. the calculated results in Fig. 5).

The magnetic field induces a separation between the two degenerate modes $\omega_\pm$, and at a finite temperature leads to a nonzero pumping current $I_{sp,x}$ along the external magnetic field. The fluctuation spin current $\langle I_{fl,x}\rangle$ is opposite to the pumping current $\langle I_{sp,x}\rangle$, and the net current $\mathbf{I}_s$ is 0 if STT is not applied ($c_J = 0$). STT can further enhance one of two thermal magnon modes and weaken the other one, generating a nonzero $\mathbf{I}_s$, see Fig. 6(b). Surprisingly, the negative current $\langle I_{s,x}\rangle$ induced by the positive c_J also increases with ω_{Hx}. When calculating the dependence of the net current $\langle I_{s,x}\rangle$ on the c_J at finite $\omega_{Hx} = 0.7$ THz, we find that the positive ω_{Hx} enhances

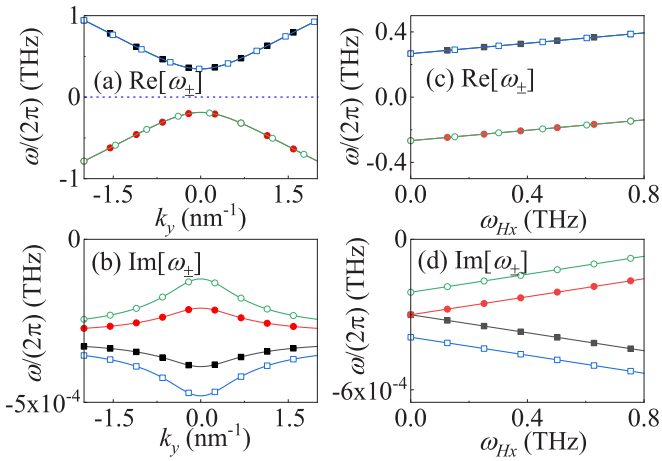

FIG. 5. (a) Dispersion relations (i.e., real parts) and (b) imaginary parts of eigenfrequencies of ω_+ (squares) and ω_- (circles) when $\omega_{Hx} = 0.1$ THz and $c_J = 0$ (solid dots) and $c_J = 0.0001$ THz (open dots). (c) Real and (d) imaginary parts of eigenfrequencies $\omega_\pm$ as functions of ω_{Hx} under $c_J = 0$ (solid dots) and $c_J = 0.0001$ THz (open dots).

the negative $\langle I_{s,x}\rangle$, while it weakens the positive $\langle I_{s,x}\rangle$, as compared to the case $\omega_{Hx} = 0$ [Fig. 3(b)]. This effect leads to an asymmetric spin pumping in AFM induced by STT and acts in favor of converting the electronic current into a magnonic spin current and vice versa.

VII. EXTERNAL MAGNETIC FIELD ALONG *y*

Under the influence of a strong magnetic field, ω_{Hx} applied along the x axis or ω_{Hy} applied along y axis, the linear antiparallel orientation of AFM magnetization loses its stability and a spin-flop transition occurs. In this case, a nonzero net magnetization builds up along the magnetic field and increases with the amplitude of the magnetic field. The equilibrium Néel order vector is perpendicular to the magnetic field. To explore the influences of the spin-flop on the net magnetization, we mainly study the case when ω_{Hy} is applied along the y axis.

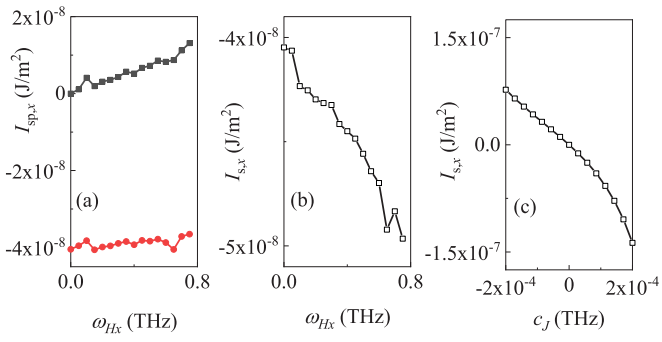

FIG. 6. For a 1D model at the temperature $T = 30$ K, (a) spin pumping spin current $\langle I_{sp,x}\rangle$ (black squares for $c_J = 0$, red circles for $c_J = 1 \times 10^{-4}$ THz) and (b) net spin current $\langle I_{s,x}\rangle$ (when $c_J = 1 \times 10^{-4}$ THz) as functions of magnetic field ω_{Hx}. (c) At $\omega_{Hx} = 0.7$ THz, c_J dependence of net current $\langle I_{s,x}\rangle$. Here, the strength of DC magnetic field H_x is given in the unit of frequency, i.e., $\omega_{Hx} = \gamma H_x$.

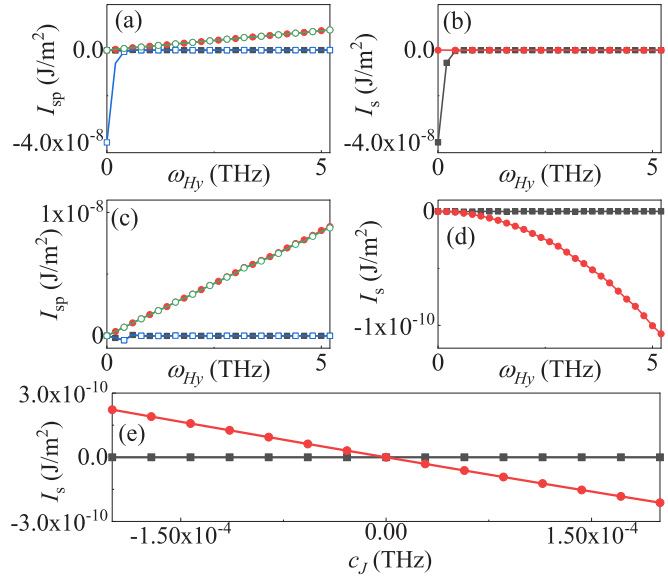

FIG. 7. For 1D model at $T = 30$ K, the x component $\langle I_{sp,x}\rangle$ (squares line) and the y component $\langle I_{sp,y}\rangle$ (circles line) of the spin pumping currents are shown as functions of the magnetic field ω_{Hy}, under $c_J = 0$ (solid dots) or $c_J = 1 \times 10^{-4}$ THz (open dots) with (a) $\boldsymbol{\mu}_s^N = \mathbf{x}$ and (c) $\boldsymbol{\mu}_s^N = \mathbf{y}$. With $c_J = 1 \times 10^{-4}$ THz and (b) $\boldsymbol{\mu}_s^N = \mathbf{x}$ and (d) $\boldsymbol{\mu}_s^N = \mathbf{y}$, the net spin currents $\langle I_{s,x}\rangle$ (squares line) and $\langle I_{s,y}\rangle$ (circles line) as functions of the magnetic field ω_{Hy}. (e) When $\omega_{Hy} = 5.2$ THz, c_J dependence of the net spin currents $\langle I_{s,x}\rangle$ (squares line) and $\langle I_{s,y}\rangle$ (circles line).

Applying positive ω_{Hy} generates a net magnetization $\mathbf{m}_0 = (0, m_{0,y}, 0)$ with $m_{0,y} > 0$. The thermal fluctuation of this net magnetization exerts a positive pumping current $\langle I_{sp,y}\rangle$ along y, as shown by Fig. 7. This behavior is similar to the features of a thermal pumping current in FM [49]. Along the x axis, the dynamics of opposite sublattice magnetizations are symmetric, and the pumping current in this case is zero $\langle I_{sp,x}\rangle = 0$. Applying STT with $\boldsymbol{\mu}_s^N = (1, 0, 0)$ only affects $\langle I_{sp,x}\rangle$, and a positive c_J drives a negative $\langle I_{sp,x}\rangle$ and hence a negative net current $\langle I_{s,x}\rangle$ [see Figs. 7(a) and 7(b)]. This effect is similar to the effect described above (Fig. 3). However, the increase in ω_{Hy} strongly weakens this effect, and $\langle I_{sp,x}\rangle$ and $\langle I_{s,x}\rangle$ approach 0 for larger ω_{Hy}. To understand this phenomenon, we also analyze the change in Im[$\omega_\pm$] induced by STT. However, this effect is negligible for lager ω_{Hy} (not shown).

Applying STT with polarization $\boldsymbol{\mu}_s^N = (0, 1, 0)$ impacts the dynamics of the net magnetization along $\mathbf{y}$. It enhances/weakens the thermal fluctuation of the net magnetization and hence $\langle I_{sp,y}\rangle$. As demonstrated in Figs. 7(c) and 7(d), the positive c_J decreases the $\langle I_{sp,y}\rangle$, generating a negative $\langle I_{s,y}\rangle$. The induced $\langle I_{s,y}\rangle$ increases with the net magnetization $m_{0,y}$ and thus magnetic field ω_{Hy}.

After reversing the sign of c_J, the current $\langle I_{s,y}\rangle$ becomes positive [Fig. 7(e)]. With further increasing of the amplitude of c_J (not shown), we observe a nonlinear variation in $\langle I_{s,y}\rangle$, where the negative $\langle I_{s,y}\rangle$ can be larger than the positive $\langle I_{s,y}\rangle$ under the same $|c_J|$. This nonlinear and asymmetric variation in the net magnetization fluctuation resembles the effect in FM [17]. Noteworthy, as compared with the case in absence of the magnetic field and $\boldsymbol{\mu}_s^N \parallel \mathbf{n}_0$, the current $\langle I_{s,y}\rangle$ is much

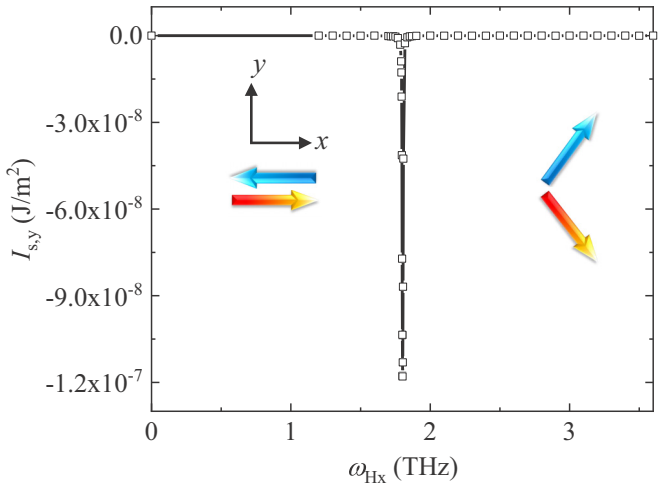

FIG. 8. The magnetic field ω_{Hx} is applied along $\mathbf{x}$ and $\boldsymbol{\mu}_s^N = \mathbf{y}$ ($c_J = 1 \times 10^{-4}$ THz). The net spin current $I_{s,y}$ as a function of ω_{Hx} has a sharp peak for the spin-flop field 1.7 THz.

smaller (cf. Fig. 3), even when the magnetic field is sufficiently strong ($\omega_{Hy} = 5.2$ THz). Based on this observation we conclude that when a finite net magnetization builds up along the external magnetic field, the induced spin pumping current is smaller than in the case of Néel order vector.

The results obtained in our work are relevant to experimental studies [36]. In particular, a large nonlocal spin signal R_{el} was detected for the Néel vector $\mathbf{n}$ oriented parallel to the electron spin polarization $\boldsymbol{\mu}_s^N$. A sharp peak was observed at the spin-flop transition point when $\mathbf{n}$ turns to the direction of $\boldsymbol{\mu}_s^N$. When $\mathbf{n}$ is perpendicular to $\boldsymbol{\mu}_s^N$, the signal R_{el} is very small. These experimental facts are in a good agreement with our theoretical results. In our case as well we find that the electron-magnon spin conversion is most efficient when $\mathbf{n}$ is parallel to $\boldsymbol{\mu}_s^N$. Besides, when the average magnetization $\mathbf{m}$ is parallel to $\boldsymbol{\mu}_s^N$, the asymmetry of pumping current I_s with respect to the direction of electric current contributes to the detected thermal signal R_{th}. The sharp peak induced by the spin accumulation at the spin-flop transition point was theoretically predicted in Ref. [41]. A similar observation of the sharp peak at the spin-flop transition point is demonstrated in Fig. 8. Below the spin-flop transition point, the pumping current is small, as $\mathbf{n}$ is perpendicular to $\boldsymbol{\mu}_s^N$. At the spin-flop transition point ($\omega_{Hx} = 1.7$ THz) where the Néel order parameter $\mathbf{n}$ aligns with the direction of $\boldsymbol{\mu}_s^N$ a sharp peak is observed. The large increase in the pumping current is related to a closing of the magnon gap of one of the modes [36,41]. The gap reopens at a higher field, and the pumping current becomes smaller again.

VIII. CONCLUSION

We studied the electron-magnon spin conversion process in a HM/AFM/HM heterostructure. A charge current in the metallic layer drives the spin dynamics in the AFM via spin transfer torque (STT) effects. Two degenerate AFM magnon modes with opposite polarization are involved. Depending on the electron polarization, STT enhances one of two modes and suppresses the other. At finite temperatures, the creation/annihilation of the two magnon modes in AFM by the STT leads to a net spin pumping current. This current increases nonlinearly with the electric current density in the HM layer. An external magnetic field can control the conversion process, which is shown to be quite efficient and potentially useful for designing antiferromagnetic-based spintronic devices.

ACKNOWLEDGMENTS

This work was supported by the National Natural Science Foundation of China (Grants No. 12074437, No. 11674400, No. 11704415, and No. 11374373), DFG through SFB 762 and SFB TRR227, and the Natural Science Foundation of Hunan Province of China (Grants No. 2018JJ3629 and No. 2020JJ4104).

[1] I. Žutić, J. Fabian, and S. Das Sarma, Rev. Mod. Phys. **76**, 323 (2004).
[2] A. V. Chumak, V. I. Vasyuchka, A. A. Serga, and B. Hillebrands, Nat. Phys. **11**, 453 (2015).
[3] S. A. Wolf, D. D. Awschalom, R. A. Buhrman, J. M. Daughton, S. von Molnár, M. L. Roukes, A. Y. Chtchelkanova, and D. M. Treger, Science **294**, 1488 (2001).
[4] H. Ohno, Nat. Mater. **9**, 952 (2010).
[5] J. Sinova, S. O. Valenzuela, J. Wunderlich, C. H. Back, and T. Jungwirth, Rev. Mod. Phys. **87**, 1213 (2015).
[6] B. Heinrich, C. Burrowes, E. Montoya, B. Kardasz, E. Girt, Y.-Y. Song, Y. Sun, and M. Wu, Phys. Rev. Lett. **107**, 066604 (2011).
[7] J. E. Hirsch, Phys. Rev. Lett. **83**, 1834 (1999).
[8] S. O. Valenzuela and M. Tinkham, Nature (London) **442**, 176 (2006).
[9] Y. K. Kato, R. C. Myers, A. C. Gossard, and D. D. Awschalom, Science **306**, 1910 (2004).
[10] Y. Tserkovnyak, A. Brataas, G. E. W. Bauer, and B. I. Halperin, Rev. Mod. Phys. **77**, 1375 (2005).
[11] E. Saitoh, M. Ueda, H. Miyajima, and G. Tatara, Appl. Phys. Lett. **88**, 182509 (2006).
[12] C. W. Sandweg, Y. Kajiwara, A. V. Chumak, A. A. Serga, V. I. Vasyuchka, M. B. Jungfleisch, E. Saitoh, and B. Hillebrands, Phys. Rev. Lett. **106**, 216601 (2011).
[13] K. Ando, S. Takahashi, J. Ieda, Y. Kajiwara, H. Nakayama, T. Yoshino, K. Harii, Y. Fujikawa, M. Matsuo, S. Maekawa, and E. Saitoh, J. Appl. Phys. **109**, 103913 (2011).
[14] K. Uchida, J. Xiao, H. Adachi, J. Ohe, S. Takahashi, J. Ieda, T. Ota, Y. Kajiwara, H. Umezawa, H. Kawai, G. E. W. Bauer, S. Maekawa, and E. Saitoh, Nat. Mater. **9**, 894 (2010).
[15] A. V. Chumak, A. A. Serga, M. B. Jungfleisch, R. Neb, D. A. Bozhko, V. S. Tiberkevich, and B. Hillebrands, Appl. Phys. Lett. **100**, 082405 (2012).
[16] Y. Kajiwara, K. Harii, S. Takahashi, J. Ohe, K. Uchida, M. Mizuguchi, H. Umezawa, H. Kawai, K. Ando, K. Takanashi,

S. Maekawa, and E. Saitoh, Nature (London) **464**, 262 (2010).
[17] X.-G. Wang, Z.-X. Li, Z.-W. Zhou, Y.-Z. Nie, Q.-L. Xia, Z.-M. Zeng, L. Chotorlishvili, J. Berakdar, and G.-H. Guo, Phys. Rev. B **95**, 020414(R) (2017).
[18] L. Chotorlishvili, Z. Toklikishvili, X.-G. Wang, V. K. Dugaev, J. Barnaś, and J. Berakdar, Phys. Rev. B **99**, 024410 (2019).
[19] X.-G. Wang, G.-H. Guo, Y.-Z. Nie, G.-F. Zhang, and Z.-X. Li, Phys. Rev. B **86**, 054445 (2012).
[20] T. Jungwirth, X. Marti, P. Wadley, and J. Wunderlich, Nat. Nanotechnol. **11**, 231 (2016).
[21] E. V. Gomonay and V. M. Loktev, Low Temp. Phys. **40**, 17 (2014).
[22] V. Baltz, A. Manchon, M. Tsoi, T. Moriyama, T. Ono, and Y. Tserkovnyak, Rev. Mod. Phys. **90**, 015005 (2018).
[23] O. Gomonay, V. Baltz, A. Brataas, and Y. Tserkovnyak, Nat. Phys. **14**, 213 (2018).
[24] M. B. Jungfleisch, W. Zhang, and A. Hoffmann, Phys. Lett. A **382**, 865 (2018).
[25] B. G. Park, J. Wunderlich, X. Martí, V. Holý, Y. Kurosaki, M. Yamada, H. Yamamoto, A. Nishide, J. Hayakawa, H. Takahashi, A. B. Shick, and T. Jungwirth, Nat. Mater. **10**, 347 (2011).
[26] S. M. Rezende, R. L. Rodríguez-Suárez, and A. Azevedo, Phys. Rev. B **93**, 014425 (2016).
[27] S. M. Rezende, R. L. Rodríguez-Suárez, and A. Azevedo, Phys. Rev. B **93**, 054412 (2016).
[28] P. Wadley, B. Howells, J. Železný, C. Andrews, V. Hills, R. P. Campion, V. Novák, K. Olejník, F. Maccherozzi, S. S. Dhesi, S. Y. Martin, T. Wagner, J. Wunderlich, F. Freimuth, Y. Mokrousov, J. Kuneš, J. S. Chauhan, M. J. Grzybowski, A. W. Rushforth, K. W. Edmonds *et al.*, Science **351**, 587 (2016).
[29] S. M. Wu, W. Zhang, Amit KC, P. Borisov, J. E. Pearson, J. S. Jiang, D. Lederman, A. Hoffmann, and A. Bhattacharya, Phys. Rev. Lett. **116**, 097204 (2016).
[30] X. Z. Chen, R. Zarzuela, J. Zhang, C. Song, X. F. Zhou, G. Y. Shi, F. Li, H. A. Zhou, W. J. Jiang, F. Pan, and Y. Tserkovnyak, Phys. Rev. Lett. **120**, 207204 (2018).
[31] H. Wang, C. Du, P. C. Hammel, and F. Yang, Phys. Rev. Lett. **113**, 097202 (2014).
[32] W. Lin, K. Chen, S. Zhang, and C. L. Chien, Phys. Rev. Lett. **116**, 186601 (2016).
[33] T. Moriyama, S. Takei, M. Nagata, Y. Yoshimura, N. Matsuzaki, T. Terashima, Y. Tserkovnyak, and T. Ono, Appl. Phys. Lett. **106**, 162406 (2015).
[34] J. Li, C. B. Wilson, R. Cheng, M. Lohmann, M. Kavand, W. Yuan, M. Aldosary, N. Agladze, P. Wei, M. S. Sherwin, and J. Shi, Nature (London) **578**, 70 (2020).
[35] P. Vaidya, S. A. Morley, J. van Tol, Y. Liu, R. Cheng, A. Brataas, D. Lederman, and E. del Barco, Science **368**, 160 (2020).
[36] R. Lebrun, A. Ross, S. A. Bender, A. Qaiumzadeh, L. Baldrati, J. Cramer, A. Brataas, R. A. Duine, and M. Kläui, Nature (London) **561**, 222 (2018).
[37] M. Dabrowski, T. Nakano, D. M. Burn, A. Frisk, D. G. Newman, C. Klewe, Q. Li, M. Yang, P. Shafer, E. Arenholz, T. Hesjedal, G. van der Laan, Z. Q. Qiu, and R. J. Hicken, Phys. Rev. Lett. **124**, 217201 (2020).
[38] T. Satoh, S.-J. Cho, R. Iida, T. Shimura, K. Kuroda, H. Ueda, Y. Ueda, B. A. Ivanov, F. Nori, and M. Fiebig, Phys. Rev. Lett. **105**, 077402 (2010).
[39] Q. Li, M. Yang, C. Klewe, P. Shafer, A. T. N'Diaye, D. Hou, T. Y. Wang, N. Gao, E. Saitoh, C. Hwang, R. J. Hicken, J. Li, E. Arenholz, and Z. Q. Qiu, Nat. Commun. **10**, 5265 (2019).
[40] L. Frangou, S. Oyarzún, S. Auffret, L. Vila, S. Gambarelli, and V. Baltz, Phys. Rev. Lett. **116**, 077203 (2016).
[41] S. A. Bender, H. Skarsvåg, A. Brataas, and R. A. Duine, Phys. Rev. Lett. **119**, 056804 (2017).
[42] R. Cheng, D. Xiao, and A. Brataas, Phys. Rev. Lett. **116**, 207603 (2016).
[43] R. Cheng, J. Xiao, Q. Niu, and A. Brataas, Phys. Rev. Lett. **113**, 057601 (2014).
[44] O. Johansen and A. Brataas, Phys. Rev. B **95**, 220408(R) (2017).
[45] L. Chotorlishvili, S. R. Etesami, J. Berakdar, R. Khomeriki, and J. Ren, Phys. Rev. B **92**, 134424 (2015).
[46] O. Johansen, H. Skarsvåg, and A. Brataas, Phys. Rev. B **97**, 054423 (2018).
[47] Y.-T. Chen, S. Takahashi, H. Nakayama, M. Althammer, S. T. B. Goennenwein, E. Saitoh, and G. E. W. Bauer, Phys. Rev. B **87**, 144411 (2013).
[48] X.-G. Wang, Z.-W. Zhou, Y.-Z. Nie, Q.-L. Xia, and G.-H. Guo, Phys. Rev. B **97**, 094401 (2018).
[49] J. Xiao, G. E. W. Bauer, K.-C. Uchida, E. Saitoh, and S. Maekawa, Phys. Rev. B **81**, 214418 (2010).
[50] R. Khymyn, I. Lisenkov, V. Tiberkevich, B. A. Ivanov, and A. Slavin, Sci. Rep. **7**, 43705 (2017).
[51] I. N. Krivorotov, N. C. Emley, J. C. Sankey, S. I. Kiselev, D. C. Ralph, and R. A. Buhrman, Science **307**, 228 (2005).
[52] L. Liu, O. J. Lee, T. J. Gudmundsen, D. C. Ralph, and R. A. Buhrman, Phys. Rev. Lett. **109**, 096602 (2012).
[53] K. Garello, I. M. Miron, C. O. Avci, F. Freimuth, Y. Mokrousov, S. Blügel, S. Auffret, O. Boulle, G. Gaudin, and P. Gambardella, Nat. Nanotechnol. **8**, 587 (2013).
[54] A. Hoffmann, IEEE Trans. Magn. **49**, 5172 (2013).